Published in final edited form as:
Cell. 2009 September 18; 138(6): 1222–1235. doi:10.1016/j.cell.2009.06.050.

Synaptic PRG-1 Modulates Excitatory Transmission via Lipid Phosphate-Mediated Signaling

Thorsten Trimbuch[1,10], **Prateep Beed**[2,10], **Johannes Vogt**[1,10], **Sebastian Schuchmann**[2], **Nikolaus Maier**[2], **Michael Kintscher**[1,2], **Jörg Breustedt**[2], **Markus Schuelke**[3], **Nora Streu**[1], **Olga Kieselmann**[1], **Irene Brunk**[4], **Gregor Laube**[4], **Ulf Strauss**[1], **Arne Battefeld**[1], **Hagen Wende**[5], **Carmen Birchmeier**[5], **Stefan Wiese**[6], **Michael Sendtner**[6], **Hiroshi Kawabe**[7], **Mika Kishimoto-Suga**[7], **Nils Brose**[7], **Jan Baumgart**[1], **Beate Geist**[1], **Junken Aoki**[8], **Nic E. Savaskan**[1], **Anja U. Bräuer**[1], **Jerold Chun**[9], **Olaf Ninnemann**[1], **Dietmar Schmitz**[2,11], and **Robert Nitsch**[1,*,11]

[1]Institute of Cell Biology and Neurobiology and NeuroCure, Universitä tsmedizin Berlin, Charité platz 1, 10117 Berlin, Germany

[2]Neuroscience Research Center and NeuroCure, Universitä tsmedizin Berlin, Charité platz 1, 10117 Berlin, Germany

[3]Department of Neuropediatrics and NeuroCure Clinical Research Center, Universitä tsmedizin Berlin, Charité platz 1, 10117 Berlin, Germany

[4]Institute of Integrative Neuroanatomy, Charité, Universitä tsmedizin Berlin, Charité platz 1, 10117 Berlin, Germany

[5]Max-Delbrück-Center for Molecular Medicine, Robert-Rössle-Str. 10, 13092 Berlin, Germany

[6]Institute of Clinical Neurobiology, Universität Würzburg, Zinklesweg 10, 97078 Würzburg, Germany

[7]Department of Molecular Neurobiology, Max Planck Institute of Experimental Medicine, Hermann-Rein-Str. 3 37075 Göttingen, Germany

[8]Graduate School of Pharmaceutical Sciences, Tohoku University, 6-3, Aoba, Aramaki, Aoba-ku, Sendai, Miyagi, 980-8578, Japan

[9]The Scripps Research Institute, 10550 North Torrey Pines Rd., La Jolla, CA 92037, USA

SUMMARY

Plasticity related gene-1 (PRG-1) is a brain-specific membrane protein related to lipid phosphate phosphatases, which acts in the hippocampus specifically at the excitatory synapse terminating on glutamatergic neurons. Deletion of prg-1 in mice leads to epileptic seizures and augmentation of EPSCs, but not IPSCs. In utero electroporation of PRG-1 into deficient animals revealed that PRG-1 modulates excitation at the synaptic junction. Mutation of the extracellular domain of PRG-1 crucial for its interaction with lysophosphatidic acid (LPA) abolished the ability to prevent hyperexcitability. As LPA application in vitro induced hyperexcitability in wild-type but not in

*Correspondence: robert.nitsch@charite.de.
[10]These authors contributed equally to this work
[11]These authors contributed equally to this work

SUPPLEMENTAL DATA
Supplemental Data include ten figures, Supplemental Experimental Procedures, and three movies and can be found with this article online at http://www.cell.com/supplemental/S0092-8674(09)00843-5.

LPA_2 receptor-deficient animals, and uptake of phospholipids is reduced in PRG-1-deficient neurons, we assessed PRG-1/LPA_2 receptor-deficient animals, and found that the pathophysiology observed in the PRG-1-deficient mice was fully reverted. Thus, we propose PRG-1 as an important player in the modulatory control of hippocampal excitability dependent on presynaptic LPA_2 receptor signaling.

INTRODUCTION

Recently, we discovered a new class of proteins, which we named plasticity-related genes (PRGs) because two members of the PRG family, PRG-1 (LPR-4) and PRG-3 (LPR-1), play a role in regulating cellular plasticity. Their actions include filopodia formation, neurite extension, axonal path finding and reorganization after lesions (Bräuer et al., 2003; Peeva et al., 2006; Savaskan et al., 2004; Sigal et al., 2007). PRGs are integral membrane proteins that possess homology to lipid phosphate phosphatases (LPPs) and can be classified as part of the superfamily of lipid phosphatases/phosphotransferases (PAP2, also known as LPT) (Sigal et al., 2005). PRG-1 bears the characteristic LPP feature of three conserved domains facing the extracellular side of the plasma membrane or the luminal side of cellular membranes (Zhang et al., 2000). These domains enable the LPPs to dephosphorylate a variety of phosphorylated lipid substrates, such as phosphatidate (PA), lysophosphatidate (LPA) or sphingosine-1-phosphate (S1P) (Brindley and Waggoner, 1998). Bioactive lipid phosphates are key factors in initiating receptor-directed signaling cascades (Anliker and Chun, 2004; Fukushima and Chun, 2001; Milstien et al., 2007) and participate in diverse cellular processes, such as cell proliferation, neurite retraction, cortical development, and regulation of exocytosis (Kingsbury et al., 2003; Moolenaar et al., 2004; Pan et al., 2007; Spiegel et al., 2002; Ye et al., 2002). Therefore, LPPs may act as negative regulators of these signaling cascades dependent on critical amino acids within the conserved domains (Brindley, 2004; McDermott et al., 2004; Neuwald, 1997; Pyne et al., 2005; Sigal et al., 2005). Interestingly, unlike other members of the PAP2 superfamily, PRG-1 contains an additional C-terminal hydrophilic domain of around 400 amino acids (Bräuer et al., 2003). We previously showed that the neuronal cell line N1E-115, when transfected with a *prg-1*-GFP fusion construct and exposed to LPA, generates increased extracellular LPA degradation products. Moreover, these cells were protected against LPA-induced neurite collapse in a dose-dependent fashion (Bräuer et al., 2003; McDermott et al., 2004), which demonstrates that PRG-1 had interfered with lipid phosphate signaling. Our studies have so far revealed that expression of *prg-1* is vertebrate- and brain-specific, and that the gene is highly conserved in vertebrate species, including humans. Expression of PRG-1 begins perinatally, is strongly expressed in hippocampal neurons and rapidly upregulated after lesion of the glutamatergic entorhinal fiber tract (Bräuer et al., 2003).

RESULTS

Neuronal Localization of PRG-1

Using an antibody against PRG-1, we found the protein exclusively in neurons, as shown by colocalization with the neuronal marker NeuN (Figure 1A). $GFAP^+$ astrocytes or microglial cells and oligodendrocytes (data not shown) were not stained (Figure 1A). Double staining and in situ hybridization showed expression of the *prg-1* gene exclusively in NeuN-containing neurons, but not in astrocytes (Figure 1B). PRG-1 did not colocalize with GABAergic markers including glutamic acid decarboxylase-67 (GAD67) or calcium-binding proteins, such as calbindin (CB), calretinin (CR) and parvalbumin (PV). Similarly, no colocalization was observed with *prg-1* mRNA by in situ hybridization (Figure 1C). PRG-1 colocalized with ProSAP2 and Homer1, molecules specifically located at the postsynaptic density of glutamatergic synapses (Brakeman et al., 1997; Tu et al., 1999;

Wouterlood et al., 2003), but not Gephyrin, a marker at the postsynaptic side of GABAergic contacts (Sassoe-Pognetto and Fritschy, 2000). Subfractionation of the synaptosomal preparation (Cotman and Taylor, 1972) showed that PRG-1 was present in the postsynaptic density (PSD), but absent in presynaptic vesicles. Finally, localization at the ultrastructural level revealed DAB-reaction product, indicating PRG-1 immunolabeling exclusively at postsynaptic structures of asymmetric synapses of CA1 pyramidal cells and silver-enhanced immunogold signal of PRG-1 bordering the synaptic cleft (Figure 1D). These data indicate that PRG-1 plays a role at the postsynaptic site of glutamatergic neurons in the hippocampus.

EEG Recordings Reveal Seizure Activity in PRG-1 KO Mice

We disrupted the *prg-1* gene by inserting an IRES-LacZ-MC1-Neo cassette, which deletes the extracellular domains coded on exons 5 and 6 and blocks translation of the intracellular tail coded by exon 7 (Figure S1 available with this article online). The PRG-$1^{-/-}$ mice were viable but showed a transiently reduced weight during development (Figure S2A), a reduction in brain weight (Figure S2B), and a mortality of approximately 50% at 3–4 weeks after birth (Figure S2C). Since we observed seizure-like movements of some PRG-$1^{-/-}$ mice around post-natal day (P) 20, we made in vivo electrographic recordings using intracranial, epidural electrodes above the somatosensory cortex in knockout (KO) and wild-type (WT) mice at P19-P31. In all investigated KO mice (n = 10), but none of the WT mice (n = 7), hypersynchronized activity and preictal events were identified by field potential shifts (>150 μV) as early as around P20 (Figure 2A). Electrographic ictal events and tonic-clonic seizures were observed in 5 of 10 KO mice over the following two days (Figures 2A–2C and Movies S1 and S2). The frequency of field potential discharges was 3–5 Hz during ictal activity and 0.8–1.6 Hz during interictal activity (Figure 2B). All recorded KO mice exhibiting electrographic seizures died during status epilepticus (ictal activity > 30 min). The KO mice with implanted electrodes at both hemispheres showed preictal events at only one, but ictal activity at both, hemispheres (KO, n = 4; WT, n = 3; Figure 2C), suggesting a focal ictogenesis with secondary generalization. In a number of KO mice only hypersynchronized activity, but no ictal events, were registered (n = 3). These in vivo recordings indicate that lack of PRG-1 results in severe alteration of synaptic transmission leading to juvenile epileptic seizures.

No Evident Structural Changes, but Pathological Network Properties in Hippocampal Slices

Surprisingly, histological and immunocytochemical studies revealed no morphological alterations in PRG-$1^{-/-}$ mice. In the hippocampus of PRG-$1^{-/-}$ mice at ~P21, pyramidal neurons had developed normally as shown by the neuronal marker NeuN (Figure 3A). Specifically, the distribution of inhibitory GABAergic interneurons expressing parvalbumin was not altered in these mice (Figure 3A). Also, synaptic innervation of CA3 and CA1 pyramidal cells was unchanged at P21 in PRG-$1^{-/-}$ mice (Figure S3). Whole-cell patch clamp experiments in current clamp mode on WT and KO mice at that age did not reveal any obvious difference in intrinsic properties of CA1 pyramidal cells that would indicate alteration of the cellular architecture of individual neurons (Figure 3B). In vitro studies of the robust network rhythms in the hippocampus (Maier et al., 2003) by analyzing sharp waves (SPW) and accompanying ripples in the CA3 area in hippocampal slices from PRG-1 KO mice at P21 (Figure 3C) revealed that SPW incidence was not altered in either condition (WT: 2.2 ± 0.2 Hz versus KO: 2.4 ± 0.6 Hz; n = 8 for both groups, Mann-Whitney Test, p = 0.44; Figure 3D). Likewise, spectral frequency and ripple power were not significantly altered in slices from WT or PRG-1 KO animals (frequency: 222.5 ± 4.5 Hz and 218.2 ± 6.8 Hz, for WT and KO, respectively; n = 8, Mann-Whitney Test, p = 0.64; ripple power: controls: 150 ± 43 μV versus 209 ± 48 μV, n = 8, Mann-Whitney Test, p = 0.44; Figure

3D). However, bath application of carbachol induced gamma oscillation in WT slices (Figure 3E) (Fisahn et al., 1998). In slices from KO animals, we additionally detected interictal discharges (~78% of tested slices; compare to data presented in Figure 3C with summary diagram in Figure 3D). These findings suggest that PRG-1 deficiency results in pathological network synchronization, probably due to a pathological increase of excitatory synaptic transmission.

Hyperexcitability in CA1 Neurons

To elucidate the mechanistic role of PRG-1 in the cellular physiology of hippocampal pyramidal neurons, we first analyzed the so-called input-output behavior in area CA1 of acute hippocampal slices around P21. fEPSPs evoked by Schaffer collateral stimulation in the stratum radiatum of the CA1 hippocampal region showed that slices from PRG-1 KO mice (n = 10) were highly hyperexcitable compared with WT litters (n = 3, paired t test for every fiber volley, $p < 0.05$) (Figure 4A). PRG-$1^{+/-}$ mice (n = 6), which show a PRG-1 expression of approximately 50% of that of WT animals, exhibited intermediate values (Figure 4A). At single-cell level, PRG-1 KO mice showed a larger synaptic current (Figure 4B) and significantly higher mEPSC frequency (KO (n = 15, 3.22 ± 0.34 Hz) compared to WT mice (n = 14, 1.79 ± 0.26 Hz); student's t test: $p < 0.01$; Figure 4C, left panel) as recorded from CA1 pyramidal cells in voltage clamp mode. However, the mEPSC amplitude did not vary significantly between PRG-1 KO and WT (Kolmogorov-Smirnov test, $p > 0.05$, WT mean = 16.63 ± 0.13 pA, KO mean = 15.6 ± 0.14 pA, Figure 4C, right panel). This effect was specific for excitatory transmission on pyramidal neurons because (1) synaptically evoked IPSCs at different stimulation strengths did not differ between WT (n = 8) and PRG-1 KO (n = 7; paired t test for every stimulation strength, not significant for all points with $p > 0.05$; Figure 4D) mice; (2) the IV-curve of inhibitory currents showed no significant difference between WT (n = 6) and PRG-1 KO (n = 5, Figure 4E) mice, and (3) mIPSC frequency (WT n = 4, 2.13 ± 0.08 Hz, KO n = 4, 1.96 ± 0.07 Hz; student's t test: $p = 0.13$; Figure 4F) and amplitude (Kolmogorov-Smirnov test, $p > 0.05$, WT mean = 13.85 ± 0.07 pA, KO mean = 13.01 ± 0.1 pA, Figure 4F, right panel) did not vary between WT and PRG-1 KO mice. These findings demonstrate that excitatory transmission in PRG-1 KO mice was significantly increased in CA1 pyramidal neurons, whereas inhibitory events were not altered.

PRG-1 Action in Single CA1 Neurons

To differentiate between network and single-cell phenotype, the *prg-1* gene was deleted in a small subset of CA1 pyramidal cells that normally express PRG-1 protein (Figure 1A). This was achieved by Cre recombinase expression, which coexpressed GFP in a PRG-1-conditional KO mouse (for construct, see Figure S4) using in utero electroporation. These animals, aged about P21, did not show any signs of seizures. We performed simultaneous recordings from GFP^+ (PRG-1 KO genotype) and GFP^- (WT genotype) CA1 pyramidal neurons in acute hippocampal slices. Stimulus-evoked EPSC amplitudes were significantly increased in KO pyramidal cells compared with WT pyramidal cells (KO (n = 7); WT (n = 7); student's t test: $p < 0.01$; Figure 5A, left). Recordings from GFP^+ and GFP^- CA1 pyramidal cells showed a significantly higher mEPSC frequency in the PRG-1-deficient pyramidal cells compared with PRG-1-expressing pyramidal cells (KO (n = 7, 4.02 ± 0.78 Hz); WT (n = 4, 1.96 ± 0.23 Hz); student's t test: $p < 0.05$; Figure 5B left). In this setting, the majority of cells expressed PRG-1, as did, consequently, the majority of afferents on a PRG-$1^{-/-}$ CA1 pyramidal cell derived from WT CA3 neurons. This indicates that the increase in neuronal excitability is due to the lack of PRG-1 at the postsynaptic side.

Next, we electroporated *prg-1* coexpressing GFP^+ into PRG-1 KO mice to analyze whether expression of PRG-1 in single neurons can rescue the pathophysiological phenotype

independently of the surrounding KO environment. Simultaneous recordings from GFP^+ ($PRG\text{-}1^+$) and GFP^- (KO genotype) CA1 pyramidal neurons in acute hippocampal slices showed significantly decreased EPSC amplitudes in PRG-1-expressing pyramidal cells compared with KO pyramidal cells ($PRG\text{-}1^+$/ GFP^+ (n = 10); KO/GFP^- (n = 10); student's t test: $p < 0.01$; Figure 5A right). mEPSC frequency was significantly reduced in the GFP^+ cells expressing PRG-1, indicating a rescued function (KO/GFP^-: n = 4, 4.01 ± 0.29 Hz; $PRG\text{-}1^+/GFP^+$: n = 5, 1.87 ± 0.08 Hz; student's t test: $p < 0.01$; Figure 5B right). These data show that lack of PRG-1 in an individual postsynaptic neuron increases its excitatory synaptic input.

No Evidence for Changes in the Postsynaptic Molecular Machinery at the Synapse

To test for changes in the molecular machinery of synaptic transmission, we analyzed presynaptic markers, such as the vesicular GABA or glutamate transporters and postsynaptic AMPA and NMDA receptors subunits. Immunofluorescent staining showed no alteration in the expression of these molecules between PRG-1 KO and their WT litters within the hippocampus at P21 (Figure 6A). Western blotting showed no changes in expression of the postsynaptic density marker PSD-95 or the glutamate receptor subunits NR-1, NR2A/B, GluR1, GluR2/3, and GluR4 at the postsynaptic density in PRG-1 KO mice compared with WT littermates (Figure 6B). We used an antibody against an extracellular epitope of GluR2 as a marker for AMPA receptors located in the dendritic membrane, which were in direct colocalization with VGlut1 as a marker for glutamatergic synapses. We could not detect any significant difference in the presence of AMPA receptors at glutamatergic synapses (Figure 6C). Finally, we studied the AMPA/NMDA ratio (Figure 6D) and changes in the holding current in postsynaptic neurons on AMPA application (Figure 6E), both of which showed no difference between WT and PRG-1 KO animals (AMPA/NMDA: n (WT) = 4, n (KO) = 8, p = 0.75; AMPA wash in: n (WT) = 4, n (KO) = 5, p = 0.53). Therefore, we concluded that lack of PRG-1 was not affecting the postsynaptic molecular machinery involved in excitatory transmission, which would have resulted in overexcitation and eventually seizure activity. Rather, we hypothesized a postpresynaptic signaling pathway that is modulated by PRG-1.

PRG-1 Interacts with Bioactive Phospholipids

Next, we assessed the potential interaction of PRG-1 with bioactive phospholipids such as LPA at the synapse. Using fluorescence-coupled phosphatidic acid, as established in expression systems by other groups (Renault et al., 2004; Roberts and Morris, 2000), uptake of fluorescence-labeled lipids was reduced by about 50% in $PRG\text{-}1^{-/-}$ neurons when compared to WT neurons in culture (n (WT) = 30, n (KO) = 38, student's t test, $p < 0.001$) (Figure 7A). We then determined whether PRG-1 modulation of excitability at glutamatergic synapses is dependent on its involvement in lipid phosphate signaling by expressing a mutated PRG-1 protein in $PRG\text{-}1^{-/-}$ animals using in utero electroporation. This protein was coexpressed with GFP^+, and point-mutated at a critical extracellular motif (H253K) known to disrupt the interaction of LPPs with lipid phosphates in the extracellular space (Bräuer et al., 2003; McDermott et al., 2004; Starz-Gaiano et al., 2001; Zhang et al., 2000). Although the protein was also detected at the plasma membrane of GFP^+ pyramidal cells at glutamatergic synapses (Figure S6), mEPSC frequency was not reduced, indicating that a functional rescue, as obtained by expression of the WT protein, was not achieved (GFP^+ (n = 8, 3.04 ± 0.29 Hz); GFP^- (n = 4, 2.96 ± 0.23 Hz); student's t test: p = 0.855; Figure 7B). Taken together, these findings suggest that the modulatory role of PRG-1 in excitatory transmission depends on its interaction with and uptake of bioactive lipids mediated by the molecule's extracellular domains.

PRG-1 Acts via LPA_2 Receptors at the Excitatory Synapse

Finally, we investigated the signaling mechanisms at the presynaptic terminal modulated by PRG-1 at the excitatory synapse. In an independent set of experiments, we directly tracked the time course of the LPA influence on mEPSCs on single CA1 pyramidal cells in slices of WT animals. Here, bath application of 10 μM LPA induced a two-fold increase in mEPSC frequency in each CA1 neuron of WT animals tested (WT: before LPA, 0.98 ± 0.20 Hz; after LPA, 1.86 ± 0.32 Hz; mean ratio LPA/baseline: 2.00 ± 0.11; n = 10; $p < 0.01$; paired student's t test; Figure 7C). In contrast, no change was detected in mIPSC frequency (Figure S7A). Moreover, in PRG-$1^{-/-}$ animals, LPA enhanced the mEPSC frequency to a mean ratio of 1.34 ± 0.08 (n = 7, $p < 0.01$). This increase, however, was significantly smaller in comparison to WT animals ($p < 0.001$, independent t test; Figure S7B).

LPA did not induce these effects in slices obtained from LPA_2 receptor (LPA_2-R)-deficient animals (LPA_2-R-KO: before LPA 0.67 ± 0.20 Hz, after LPA 0.64 ± 0.21 Hz; mean ratio LPA/baseline: 0.96 ± 0.09; n = 6; $p = 0.43$; Figure 7C). We also assessed the presence of the LPA_2-R in the hippocampus using a specific antibody (Shida et al., 2004; Figure S8A). By means of confocal triple labeling (Figure 7D), we identified specific expression of LPA_2 receptors in presynaptic terminals of the glutamatergic synapse due to its colocalization with Munc 13-1, a marker for the active zone at the presynaptic membrane (Varoqueaux et al., 2002), and VGlut-1, a marker for vesicles of the glutamatergic bouton (Takamori et al., 2000; Figures 7D and S8B). Immunostaining for LPA_2-R was found in presynaptic terminals of an asymmetric, glutamatergic junction, while symmetric, GABAergic synapses in the direct vicinity were not labeled (Figure 7E). As final proof of our hypothesis, we studied excitatory events in PRG-1/LPA_2–R $^{-/-}$ mice. fEPSPs evoked by Schaffer collateral stimulation in the stratum radiatum of the CA1 hippocampal region from double-deficient mice (n = 7) were not hyperexcitable in comparison to slices from WT litters (n = 3, paired t test for every fiber volley, $p > 0.05$), which was in contrast to findings in single PRG-$1^{-/-}$ animals (Figures 7F and 4A). On single-cell level, mEPSCs from CA1 pyramidal cells showed a significantly reduced frequency in PRG-1/LPA_2–R $^{-/-}$ mice (n = 7, 1.60 ± 0.13 Hz) compared to that of PRG-$1^{-/-}$ mice (n = 8, 3.48 ± 0.22 Hz; student's t test: $p < 0.001$; Figure 7F), which was in the range of WT animals (see Figure 4C). These double-deficient animals showed neither reduced body weight during the postnatal phase nor seizure-like behavior or increased mortality around P21 as seen in PRG-$1^{-/-}$ mice (Figure S2A, S9). Finally, in vivo EEG-recordings revealed that, unlike single PRG-1 KO mice, double-deficient animals showed no signs of epileptic discharge around P21 (Figure 7G and Movie S3; n = 4). These experiments demonstrated that changes to hippocampal network excitability, increase in glutamatergic transmission and seizure activity are fully reverted in the absence of the LPA_2-R.

DISCUSSION

Our results show that deletion of the LPP-related molecule PRG-1 results in severe hippocampal overexcitability and leads to epileptic discharge in juvenile animals. This is due to a specific role of PRG-1 at the excitatory synapse on glutamatergic neurons, which appears to be dependent on the interaction between PRG-1 and lipid phosphates such as LPA, able to signal to presynaptic LPA_2–receptors. These data indicate a scenario for the regulation of glutamatergic transmission controlled by PRG-1, which involves mechanisms mediated by bioactive lipids such as LPA and supplements the classical molecular machinery at the synapse.

PRG-1 expression on dendrites is limited to glutamatergic neurons and reaches maximum levels in the third week of life (data not shown), a time when synaptogenesis peaks and neuronal connections are shaped. In parallel, expression of LPA_2–receptors is high (Contos

and Chun, 2000; Contos et al., 2000) at this critical period of seizure susceptibility/increased hyperexcitability (Ben-Ari et al., 2007), in which an imbalance between excitatory and inhibitory inputs in the almost developed neurons is believed to occur (Ben-Ari, 2006). The lack of apparent morphological changes in PRG-1 KO animals, and specifically the presence of GABAergic neurons as in WT animals, indicated that changes in network properties were due to a pathological increase of excitatory synaptic transmission on otherwise unaffected neurons. Field potential recordings of hippocampal slices confirmed this, showing increased excitability in PRG-1 KO mice while intrinsic properties of the CA1 neurons and the overall morphology were not altered.

The fact that PRG-$1^{-/-}$ CA1 pyramidal cells showed a significantly higher stimulus-evoked EPSC amplitude and increased mEPSC frequency while neither the stimulus-evoked IPSC amplitude nor mIPSCs were affected by *prg-1* deletion indicates specific changes to glutamatergic transmission at the synapse. However, future studies are required to determine whether glutamatergic synapses outside the hippocampus are also altered. Our rescue of normal excitatory events in single PRG-$1^{-/-}$ cells by PRG-1 in utero electroporation demonstrates PRG-1's effect on neuronal excitability at individual glutamatergic synapses. In turn, deletion of *prg-1* in single cells of conditional PRG-1 KO mice using Cre-recombinase in utero electroporation was sufficient to elicit the synaptic dysfunction. Thus, our data reveal that hyperexcitability in PRG-1 KO animals can only be explained by the lack of the modulatory activity of PRG-1 at the synapse. As this single-cell KO approach never resulted in epileptic discharge in the animals and the recorded PRG-1 KO neurons were connected by normal presynaptic afferents deriving from PRG-1-expressing cells, these findings confirm that PRG-1 influences excitatory transmission from the postsynaptic side. Additionally, AMPA receptors at glutamatergic synapses and their physiological function appeared to be normal. Therefore, increased excitation at glutamatergic synapse, so far studied in CA1 and CA3 (data not shown) in vitro, and related hyperexcitability and seizures in vivo, both caused by lack of postsynaptic PRG-1, could not be explained by alteration in synaptic innervation or changes to postsynaptic receptors.

Thus, we addressed a direct role of PRG-1 in terms of its relation to lipid phosphate phosphatases. LPPs have been proposed as negative regulators of receptor-directed signaling cascades induced by bioactive lipid phosphates such as LPA or S1P (Brindley, 2004; Sigal et al., 2005). However, little is known about the physiological role of these molecules in the living organism, particularly the brain. A function for germ cell migration of one class of LPP homologs in vivo has been inferred from deletion and ectopic expression experiments in *Drosophila* (Renault et al., 2004; Starz-Gaiano et al., 2001). Homology of the membrane-spanning N-terminal part of PRG-1 to the LPP family clearly indicates their evolutionary relationship and implies that the binding partner or ligand of PRG-1 is a bioactive lipid such as LPA (Todd et al., 2002). PRG-1 and LPPs share amino acids shown to be crucial for the interaction of those molecules with lipid phosphates. In particular, mutation of a highly conserved histidine within the extracellular domain is known to abolish this interaction (Starz-Gaiano et al., 2001; Zhang et al., 2000). Precisely this exchange from histidine to lysine, when performed in PRG-1 at position 253, resulted in a protein no longer able to rescue the KO phenotype after in utero electroporation. These data support the hypothesis that PRG-1 can interfere with glutamatergic signal transduction by interacting with lipid phosphates in the synaptic cleft from the postsynaptic side (Figure S10).

Interestingly, the observed hyperexcitability in PRG-1 KO mice was gene dose-dependent with heterozygous mice showing input-output curves halfway between PRG-1-deficient and WT litters. This approximately linear relationship between protein expression and its electrophysiological action argues against an enzymatic function of PRG-1. Moreover, PRG-1 contains several nonconservative substitutions in the extracellular domains involved

in catalysis in other LPP family members, which should hamper a relevant enzymatic activity of PRG-1 in vivo (McDermott et al., 2004). In the present study, we detected that lack of PRG-1 in neurons significantly limits uptake of bioactive lipids. Therefore, there is reason to assume that apart from its potential residual enzymatic activity (Bräuer et al., 2003), PRG-1 is effective in controlling the levels of LPA at the synapse by nonenzymatic mechanisms. Thus, PRG-1 function may have evolved away from classical dephosphorylation performed by LPPs to mechanisms such as “sensor-like” or receptor/transporter-like activities. This has been shown for members of other enzyme families that have functions different to those of enzymatic relatives due to mutations in critical catalytic residues in active sites (Todd et al., 2002).

The LPA_2 receptor’s presynaptic location at the excitatory junction and the fact that LPA does not increase excitability in LPA_2 receptor-deficient mice suggests this bioactive phospholipid is directly involved in controlling glutamatergic transmission. Consequently, the absence of both overexcitation at the synapse and epileptic activity in PRG-1/LPA_2 receptor-deficient mice indicate PRG-1 modulates LPA-mediated control of excitatory discharge via the LPA_2 receptor. Changes in lipid phosphate species have been linked to forms of human epilepsy (Hermansson et al., 2005). Receptors for lipid phosphates have been described (Fukushima and Chun, 2001) as acting via G proteins and are putative transducers of a signal mediated by bioactive lipids at the synapse. Furthermore, it has been reported that lipid phosphates and their receptors can interfere with excitability (MacLennan et al., 2001) and exocytosis via G protein-coupled receptor-mediated signaling pathways (Pan et al., 2007). This indicates that modulation of neuronal transmission might involve bioactive lipids such as LPA acting via presynaptic LPA_2 receptors, a mechanism that is in turn controlled by PRG-1 from the postsynaptic side specifically at the glutamatergic junction.

EXPERIMENTAL PROCEDURES

Generation of the Mouse Lines

Constitutive PRG-1 KO mice were generated by replacing exons 4 to 5 of *prg-1* with an IRES-β-Gal-Neo cassette. Conditional PRG-1 KO mice were generated by flanking exons 4 to 6 of *prg-1* with *LoxP* sites, allowing removal by Cre recombinase expression. (see Supplemental Data). To generate a PRG-1/LPA_2 receptor$^{-/-}$ mouse line, heterozygous constitutive PRG-1 KO mice were bred with the LPA_2-R mouse line, provided by J. Chun (Contos et al., 2002).

Immunohistochemistry and DIG In Situ Hybridization

Mice were anesthetized (0.5% ketamine i.p.) and transcardially perfused with 4% PFA for IHC and DIG in situ. Brains were postfixed overnight in 4% PFA and further processed. Primary neurons or vibratome sections were blocked for 1 hr (5% normal goat serum and 0.1% Triton X-100) before overnight incubation with primary antibodies (see Supplemental Data). Sections were immunostained with Alexa-labeled secondary antibodies (Invitrogen) or with biotinylated secondary antibodies (Vector Laboratories). Ultrastructural analysis was performed as described (Krauss et al., 2007; Lujan et al., 1997). DIG in situ hybridization was performed according to manufacturer recommendations (Roche Applied Sciences) using a 400 bp DNA fragment from exon 7.

Quantitative Analysis of GluR2

Analysis of synaptic GluR2 was performed using antibodies against an extra-cellular epitope (1:300 Chemicon [Rouach et al., 2005]) and against VGlut1 (1:1000; Synaptic Systems). Colocalization of GluR2 and VGlut1 along the dendrites of CA1 neurons was analyzed by

stereological methods. Briefly, from each slice two optical sections (1 μm apart) were analyzed using an unbiased counting frame. Colocalized GluR2 and VGlut1 punctae were only counted if also present in the lower optical section as described (Mokin and Keifer, 2006).

Electrophysiology

We performed in vitro experiments, approved by the Berlin state government (T0100/03), on slices of mice (21–28 days). Mice were briefly anesthetized with isofluorane and decapitated. Brains were rapidly removed and transferred to cooled (~1°C–4°C) oxygenated artificial cerebrospinal fluid (ACSF), containing (in mM): NaCl (87), $NaHCO_3$ (26), sucrose (75), glucose (25), KCl (2.4), NaH_2PO_4 (1.25), $MgCl_2$ (7), and $CaCl_2$ (0.5); (pH 7.4). Horizontal hippocampal slices (300 μm; 400 μm for oscillation experiments) were cut on a Leica VT 1200 Vibratome (Leica Microsystems, Germany). Slices were then incubated at 34°C–35°C for 30 min or transferred to an interface-type recording chamber for oscillation experiments. All recordings were performed in ACSF containing (in mM): NaCl (119), $NaHCO_3$ (26), glucose (10), KCl (2.5), NaH_2PO_4 (1.25), $MgCl_2$ (1.3) and $CaCl_2$ (2.5), at room temperature (31°C–33°C for interface chamber experiments). All ACSF solutions were equilibrated with 95% O2 and 5% CO2; osmolarity of ACSF for recordings was maintained in the range of 290 and 305 mosmol/l. Extracellular and whole-cell patch clamp recordings in vitro were performed at 32 ± 1°C in either a submerged or interface-type recording chamber. For these recordings, we used borosilicate glass electrodes (2–5 MΩ) filled with (mM): K-gluconate (135), HEPES (10), Mg-ATP (2), KCl (20), EGTA (0.2); pH of the intracellular solution was adjusted to 7.2 with KOH. For extracellular recordings, glass microelectrodes with a tip diameter of ~5 μm were filled with ACSF before use. In some interface experiments, tungsten wire electrodes were used to sample hippocampal oscillations. Principal cells located in the pyramidal cell layer were identified using infrared differential interference contrast video microscopy. In the whole-cell configuration, de- and hyperpolarizing current steps (200 ms) were applied to characterize the cells' intrinsic properties; only cells that showed typical spiking characteristics of principal neurons were considered. Series resistance (Rs) was monitored throughout experiments; cells were rejected if Rs was > 20 MΩ or varied > ± 30% during the recording. No Rs compensation was used. Extracellular signal was amplified 1000x and filtered at 1 Hz to 2 or 5 kHz. All collected signals were digitized with 16-bit resolution (National Instruments, Austin, USA) and sampled at 5 or 10 kHz using Igor Pro (Wavemetrics, Lake Oswego, USA).

For electrographic recordings of cortical activity in vivo, teflon-coated silver wire (uncoated diameter 75 μm; Goodfellow, UK) implanted at P17 or P18 was used. The extracellular field signals were amplified 1000x (EXT 10-2F, npi, Germany) and sampled at 3 kHz using a 16-bit data acquisition board Power-Lab (8/30, ADInstruments, Spechbach, Germany) and the software Chart 5 Pro (Version 5.5.6, ADInstruments). Data were offline high-pass filtered at 45 Hz (for details see Supplemental Data).

In Utero Electroporation

The in utero electroporation experiments were carried out as described (Prozorovski et al., 2008), in accordance with a protocol approved by the local animal welfare committee. Briefly, we used time-pregnant mice at E15–E16 (post coitum). The uterine horns of anesthetized mice were exposed and the DNA solution was injected through the uterine wall into the lateral ventricle of two of the embryos. Five 38 V pulses of 50 ms were applied at 950 ms intervals by holding the injected brain with forcep-type electrodes connected to a square–pulse generator (CUY 21 Edit, Unique Medical Imada, Miyagi, Japan).

Phospholipid Uptake Experiment

Lipid uptake assays and visualization of fluorescent PA in fixed primary neurons were performed using minor modifications of described methods (Renault et al., 2004; Roberts and Morris, 2000). Primary hippocampal neurons of WT and PRG-1 KO mice were prepared from embryonic day 18 mice as described (Brandt et al., 2007). After 7 days in vitro neurons were washed in serum-free culture medium and incubated with lipid vesicles composed of 20:5 1-palmitoyl-2-oleoyl-sn-glycero-3-phosphocholine (PC) / 1-hexanoyl-2-[6-[(7-nitro-2-1,3-benzoxadiazol-4-yl)amino]hexanoyl]-sn-glycero-3-phosphate (NBD-PA) (10 μM total) (Avanti Polar Lipids, Alabaster, U.S.A.) for 5 min at 37°C. Then the cells were placed on ice, washed once with PBS and fixed for 20 min with cold 4% paraformaldehyde and mounted in antifade reagent. Fluorescent neurons of WT and PRG-1 KO were scanned with a Leica confocal laser-scanning microscope (SL) equipped with an Argon laser (excitation line 488 nm) and 40x oil objective (4x zoom). Same beam path configurations for both WT and KO cells were employed. Fluorescent images were quantified using ImageJ. Resulting mean values of fluorescent intensity were normalized to WT.

Pharmacological Compounds

Carbachol, D-APV, TTX and GABAzine were added from aqueous stock solutions; cyclothiazide and NBQX were administered from stock solutions dissolved in DMSO (final concentration of DMSO < 0.1%). All drugs were purchased from Tocris/BioTrends GmbH or Biozol GmbH (Enching, Germany) and Sigma-Aldrich. A 2.6 mM LPA stock solution was prepared by dissolving LPA (Sigma-Aldrich, Munich, Germany) in 50 mM HEPES, 138 mM NaCl, 2.7 mM KCl, 1 mM $CaCl_2$, 1mM $MgCl_2$ and 1% BSA and subsequently diluted in ACSF.

Data and Statistical Analysis

Data analysis was performed using SigmaPlot (Systat Software Inc., San Jose, USA), GraphPad Prism 4 (Graph Pad Software, La Jolla, USA) and Matlab (The Mathworks, Aachen, Germany). Spontaneous miniature EPSCs/IPSCs were detected using a threshold algorithm generated in Matlab. For calculating AMPA/NMDA ratio, the NMDA current was measured by holding the cell at +40 mV. 100 ms after the stimulus artifact, the amplitude was read off as the NMDA component. SPW-R detection was based on a voltage-threshold (>3.5SD of event-free baseline; see Supplemental Data). PSD was computed in Matlab using Thomson's multi-tapering method with adequate window and overlap values (Thomson, 1982). To detect electrographic seizure activity in vivo we used a detection threshold to define the time point when the ictal activity reached an amplitude > 3SD of activity during baseline. Data are reported as mean ± SEM, which are also presented as error bars in the figures. Statistical significance was assessed using student's t test, Kolmogorov-Smirnov test, Wilcoxon's signed rank test or the Mann-Whitney U-test for paired or unpaired data at the given significance level (p).

Supplementary Material

Refer to Web version on PubMed Central for supplementary material.

Acknowledgments

The authors thank James Ari Liebkowsky for correcting the manuscript; Denis Lajkó, Katja Rösler, Berit Söhl-Kielczynski, and Bernd Hesse-Niessen for technical assistance; and Franz Theuring for providing the IRES-LacZ-MC1-Neo cassette. This work was supported by the DFG: SFB 665/B3 to R.N., SFB 665/Z to C.B., and grant MH51699 (National Institutes of Health) to J.C. Bettina Holtmann, Elvira Rhode, Katja Becker, and Boris Jerchow are acknowledged for their help with embryonic stem cell work and blastocyst injection. T.T. and P.B. are fellows

of the GRK 1123. S.W. is now at Molecular Cell Biology Group, Ruhr-Universität Bochum, 44801 Bochum, Germany, but work was performed in the lab of M.S. and was supported by the DFG: SFB 581/B1 and Z4 to M.S.

References

Anliker B, Chun J. Cell surface receptors in lysophospholipid signaling. Semin Cell Dev Biol. 2004; 15:457–465. [PubMed: 15271291]

Ben-Ari Y. Basic developmental rules and their implications for epilepsy in the immature brain. Epileptic Disord. 2006; 8:91–102. [PubMed: 16793570]

Ben-Ari Y, Gaiarsa JL, Tyzio R, Khazipov R. GABA: a pioneer transmitter that excites immature neurons and generates primitive oscillations. Physiol Rev. 2007; 87:1215–1284. [PubMed: 17928584]

Brakeman PR, Lanahan AA, O'Brien R, Roche K, Barnes CA, Huganir RL, Worley PF. Homer: a protein that selectively binds metabotropic glutamate receptors. Nature. 1997; 386:284–288. [PubMed: 9069287]

Brandt N, Franke K, Rasin MR, Baumgart J, Vogt J, Khrulev S, Hassel B, Pohl EE, Sestan N, Nitsch R, Schumacher S. The neural EGF family member CALEB/NGC mediates dendritic tree and spine complexity. EMBO J. 2007; 26:2371–2386. [PubMed: 17431398]

Bräuer AU, Savaskan NE, Kuhn H, Prehn S, Ninnemann O, Nitsch R. A new phospholipid phosphatase, PRG-1, is involved in axon growth and regenerative sprouting. Nat Neurosci. 2003; 6:572–578. [PubMed: 12730698]

Brindley DN. Lipid phosphate phosphatases and related proteins: signaling functions in development, cell division, and cancer. J Cell Biochem. 2004; 92:900–912. [PubMed: 15258914]

Brindley DN, Waggoner DW. Mammalian lipid phosphate phosphohydrolases. J Biol Chem. 1998; 273:24281–24284. [PubMed: 9733709]

Contos JJ, Chun J. Genomic characterization of the lysophosphatidic acid receptor gene, lp(A2)/Edg4, and identification of a frameshift mutation in a previously characterized cDNA. Genomics. 2000; 64:155–169. [PubMed: 10729222]

Contos JJ, Ishii I, Chun J. Lysophosphatidic acid receptors. Mol Pharmacol. 2000; 58:1188–1196. [PubMed: 11093753]

Contos JJ, Ishii I, Fukushima N, Kingsbury MA, Ye X, Kawamura S, Brown JH, Chun J. Characterization of lpa(2) (Edg4) and lpa(1)/lpa(2) (Edg2/Edg4) lysophosphatidic acid receptor knockout mice: signaling deficits without obvious phenotypic abnormality attributable to lpa(2). Mol Cell Biol. 2002; 22:6921–6929. [PubMed: 12215548]

Cotman CW, Taylor D. Isolation and structural studies on synaptic complexes from rat brain. J Cell Biol. 1972; 55:696–711. [PubMed: 4656707]

Fisahn A, Pike FG, Buhl EH, Paulsen O. Cholinergic induction of network oscillations at 40 Hz in the hippocampus in vitro. Nature. 1998; 394:186–189. [PubMed: 9671302]

Fukushima N, Chun J. The LPA receptors. Prostaglandins Other Lipid Mediat. 2001; 64:21–32. [PubMed: 11324705]

Hermansson M, Käkelä R, Berghall M, Lehesjoki AE, Somerharju P, Lahtinen U. Mass spectrometric analysis reveals changes in phospholipid, neutral sphingolipid and sulfatide molecular species in progressive epilepsy with mental retardation, EPMR, brain, a case study. J Neurochem. 2005; 95:609–617. [PubMed: 16086686]

Kingsbury MA, Rehen SK, Contos JJ, Higgins CM, Chun J. Non-proliferative effects of lysophosphatidic acid enhance cortical growth and folding. Nat Neurosci. 2003; 6:1292–1299. [PubMed: 14625558]

Krauss M, Weiss T, Langnaese K, Richter K, Kowski A, Veh RW, Laube G. Cellular and subcellular rat brain spermidine synthase expression patterns suggest region-specific roles for polyamines, including cerebellar pre-synaptic function. J Neurochem. 2007; 103:679–693. [PubMed: 17635671]

Lujan R, Roberts JD, Shigemoto R, Ohishi H, Somogyi P. Differential plasma membrane distribution of metabotropic glutamate receptors mGluR1 alpha, mGluR2 and mGluR5, relative to neurotransmitter release sites. J Chem Neuroanat. 1997; 13:219–241. [PubMed: 9412905]

MacLennan AJ, Carney PR, Zhu WJ, Chaves AH, Garcia J, Grimes JR, Anderson KJ, Roper SN, Lee N. An essential role for the H218/AGR16/Edg-5/LP(B2) sphingosine 1-phosphate receptor in neuronal excitability. Eur J Neurosci. 2001; 14:203–209. [PubMed: 11553273]

Maier N, Nimmrich V, Draguhn A. Cellular and network mechanisms underlying spontaneous sharp wave-ripple complexes in mouse hippocampal slices. J Physiol. 2003; 550:873–887. [PubMed: 12807984]

McDermott MI, Sigal YJ, Sciorra VA, Morris AJ. Is PRG-1 a new lipid phosphatase? Nat Neurosci. 2004; 7:789. [PubMed: 15280885]

Milstien S, Gude D, Spiegel S. Sphingosine 1-phosphate in neural signalling and function. Acta Paediatr Suppl. 2007; 96:40–43. [PubMed: 17391440]

Mokin M, Keifer J. Quantitative analysis of immunofluorescent punctate staining of synaptically localized proteins using confocal microscopy and stereology. J Neurosci Methods. 2006; 157:218–224. [PubMed: 16740315]

Moolenaar WH, van Meeteren LA, Giepmans BN. The ins and outs of lysophosphatidic acid signaling. Bioessays. 2004; 26:870–881. [PubMed: 15273989]

Neuwald AF. An unexpected structural relationship between integral membrane phosphatases and soluble haloperoxidases. Protein Sci. 1997; 6:1764–1767. [PubMed: 9260289]

Pan CY, Wu AZ, Chen YT. Lysophospholipids regulate excitability and exocytosis in cultured bovine chromaffin cells. J Neurochem. 2007; 102:944–956. [PubMed: 17630986]

Peeva GP, Angelova SK, Guntinas-Lichius O, Streppel M, Irintchev A, Schutz U, Popratiloff A, Savaskan NE, Brauer AU, Alvanou A, et al. Improved outcome of facial nerve repair in rats is associated with enhanced regenerative response of motoneurons and augmented neocortical plasticity. Eur J Neurosci. 2006; 24:2152–2162. [PubMed: 17074041]

Prozorovski T, Schulze-Topphoff U, Glumm R, Baumgart J, Schroter F, Ninnemann O, Siegert E, Bendix I, Brustle O, Nitsch R, et al. Sirt1 contributes critically to the redox-dependent fate of neural progenitors. Nat Cell Biol. 2008; 10:385–394. [PubMed: 18344989]

Pyne S, Long JS, Ktistakis NT, Pyne NJ. Lipid phosphate phosphatases and lipid phosphate signalling. Biochem Soc Trans. 2005; 33:1370–1374. [PubMed: 16246121]

Renault AD, Sigal YJ, Morris AJ, Lehmann R. Soma-germ line competition for lipid phosphate uptake regulates germ cell migration and survival. Science. 2004; 305:1963–1966. [PubMed: 15331773]

Roberts RZ, Morris AJ. Role of phosphatidic acid phosphatase 2a in uptake of extracellular lipid phosphate mediators. Biochim Biophys Acta. 2000; 1487:33–49. [PubMed: 10962286]

Rouach N, Byrd K, Petralia RS, Elias GM, Adesnik H, Tomita S, Karimzadegan S, Kealey C, Bredt DS, Nicoll RA. TARP gamma-8 controls hippocampal AMPA receptor number, distribution and synaptic plasticity. Nat Neurosci. 2005; 8:1525–1533. [PubMed: 16222232]

Sassoe-Pognetto M, Fritschy JM. Mini-review: gephyrin, a major postsynaptic protein of GABAergic synapses. Eur J Neurosci. 2000; 12:2205–2210. [PubMed: 10947798]

Savaskan NE, Brauer AU, Nitsch R. Molecular cloning and expression regulation of PRG-3, a new member of the plasticity-related gene family. Eur J Neurosci. 2004; 19:212–220. [PubMed: 14750979]

Shida D, Watanabe T, Aoki J, Hama K, Kitayama J, Sonoda H, Kishi Y, Yamaguchi H, Sasaki S, Sako A, et al. Aberrant expression of lysophosphatidic acid (LPA) receptors in human colorectal cancer. Lab Invest. 2004; 84:1352–1362. [PubMed: 15220934]

Sigal YJ, McDermott MI, Morris AJ. Integral membrane lipid phosphatases/phosphotransferases: common structure and diverse functions. Biochem J. 2005; 387:281–293. [PubMed: 15801912]

Sigal YJ, Quintero OA, Cheney RE, Morris AJ. Cdc42 and ARP2/3-independent regulation of filopodia by an integral membrane lipidphosphatase-related protein. J Cell Sci. 2007; 120:340–352. [PubMed: 17200142]

Spiegel S, English D, Milstien S. Sphingosine 1-phosphate signaling: providing cells with a sense of direction. Trends Cell Biol. 2002; 12:236–242. [PubMed: 12062172]

Starz-Gaiano M, Cho NK, Forbes A, Lehmann R. Spatially restricted activity of a Drosophila lipid phosphatase guides migrating germ cells. Development. 2001; 128:983–991. [PubMed: 11222152]

Takamori S, Rhee JS, Rosenmund C, Jahn R. Identification of a vesicular glutamate transporter that defines a glutamatergic phenotype in neurons. Nature. 2000; 407:189–194. [PubMed: 11001057]

Thomson DJ. Spectrum estimation and harmonic analysis. Proc IEEE. 1982; 70:1055–1096.

Todd AE, Orengo CA, Thornton JM. Sequence and structural differences between enzyme and nonenzyme homologs. Structure. 2002; 10:1435–1451. [PubMed: 12377129]

Tu JC, Xiao B, Naisbitt S, Yuan JP, Petralia RS, Brakeman P, Doan A, Aakalu VK, Lanahan AA, Sheng M, Worley PF. Coupling of mGluR/Homer and PSD-95 complexes by the Shank family of postsynaptic density proteins. Neuron. 1999; 23:583–592. [PubMed: 10433269]

Varoqueaux F, Sigler A, Rhee JS, Brose N, Enk C, Reim K, Rosenmund C. Total arrest of spontaneous and evoked synaptic transmission but normal synaptogenesis in the absence of Munc13-mediated vesicle priming. Proc Natl Acad Sci USA. 2002; 99:9037–9042. [PubMed: 12070347]

Wouterlood FG, Bockers T, Witter MP. Synaptic contacts between identified neurons visualized in the confocal laser scanning microscope. Neuroanatomical tracing combined with immunofluorescence detection of post-synaptic density proteins and target neuron-markers. J Neurosci Methods. 2003; 128:129–142. [PubMed: 12948556]

Ye X, Fukushima N, Kingsbury MA, Chun J. Lysophosphatidic acid in neural signaling. Neuroreport. 2002; 13:2169–2175. [PubMed: 12488791]

Zhang QX, Pilquil CS, Dewald J, Berthiaume LG, Brindley DN. Identification of structurally important domains of lipid phosphate phosphatase-1: implications for its sites of action. Biochem J. 2000; 345:181–184. [PubMed: 10620492]

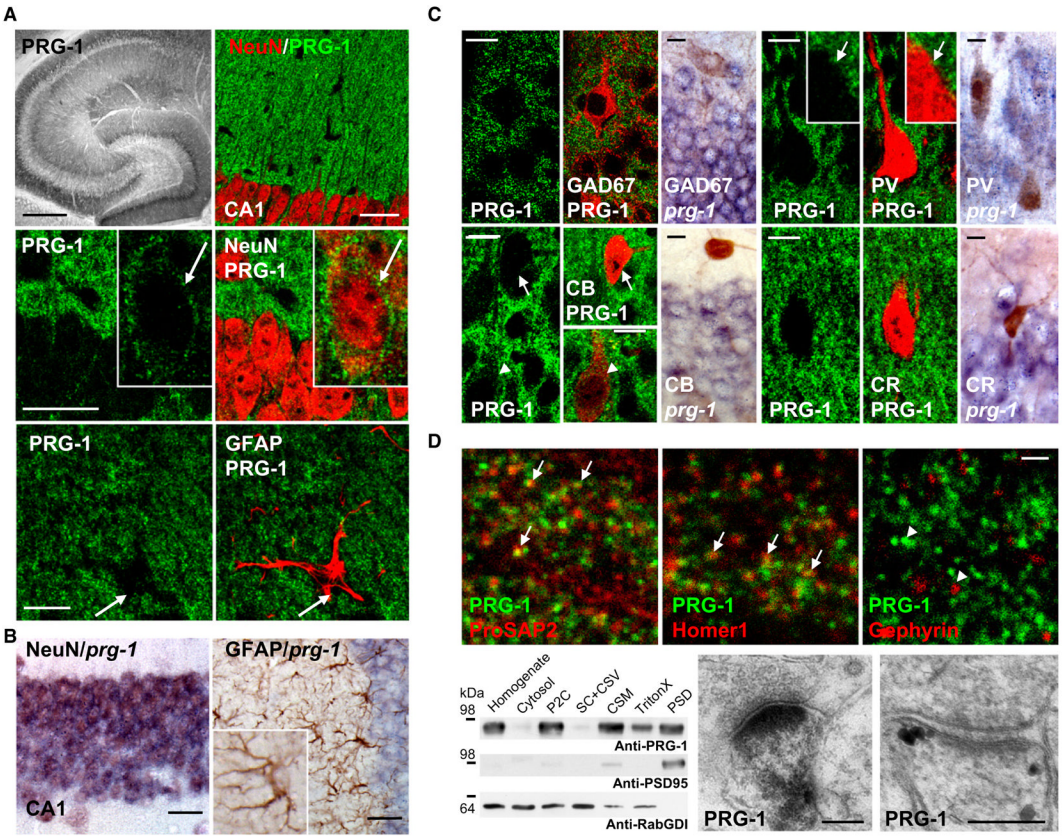

Figure 1. PRG-1 Is a Neuronal, Synaptic Molecule Expressed by Glutamatergic Neurons

(A) PRG-1 expression in the adult hippocampus as shown by immunohistochemistry (the scale bar represents 250 μm on the left, and 50 μm on the right, respectively). Dendrites of CA1 pyramids exhibit high expression, with membrane-bound expression shown in higher magnification (insets, arrows). PRG-1 did not colocalize with glial markers such as GFAP (the scale bar represents 15 μm).

(B) In situ hybridization of *prg-1* colocalized with the neuronal marker NeuN but not with $GFAP^+$ cells in the CA1 region (the scale bar represents 50 μm).

(C) PRG-1/*prg-1* was not expressed in interneurons as shown for GAD67, Parvalbumin (PV, arrows), Calbindin (CB, arrows) and Calretinin (CR) by immune stainings and in situ hybridization but was expressed in CB+ CA1 pyramids (arrowheads) (the scale bar represents 15 μm).

(D) PRG-1 was mainly expressed on dendrites and colocalized with ProSAP2 and Homer, but not Gephyrin (the scale bar represents 2 μm). Subcellular fractionation of mouse cerebral cortex revealed PRG-1 within the PSD. RabGDI was slightly enriched in the SC +CSV fraction but undetectable in the PSD-95 enriched PSD fraction, whereas PRG-1 was detected in this fraction but not in the presynaptic vesicle fraction (SC+CSV). Ultrastructural analysis of PRG-1 expression shows preferential expression of PRG-1 at the postsynaptic density (the scale bar represents 200 nm).

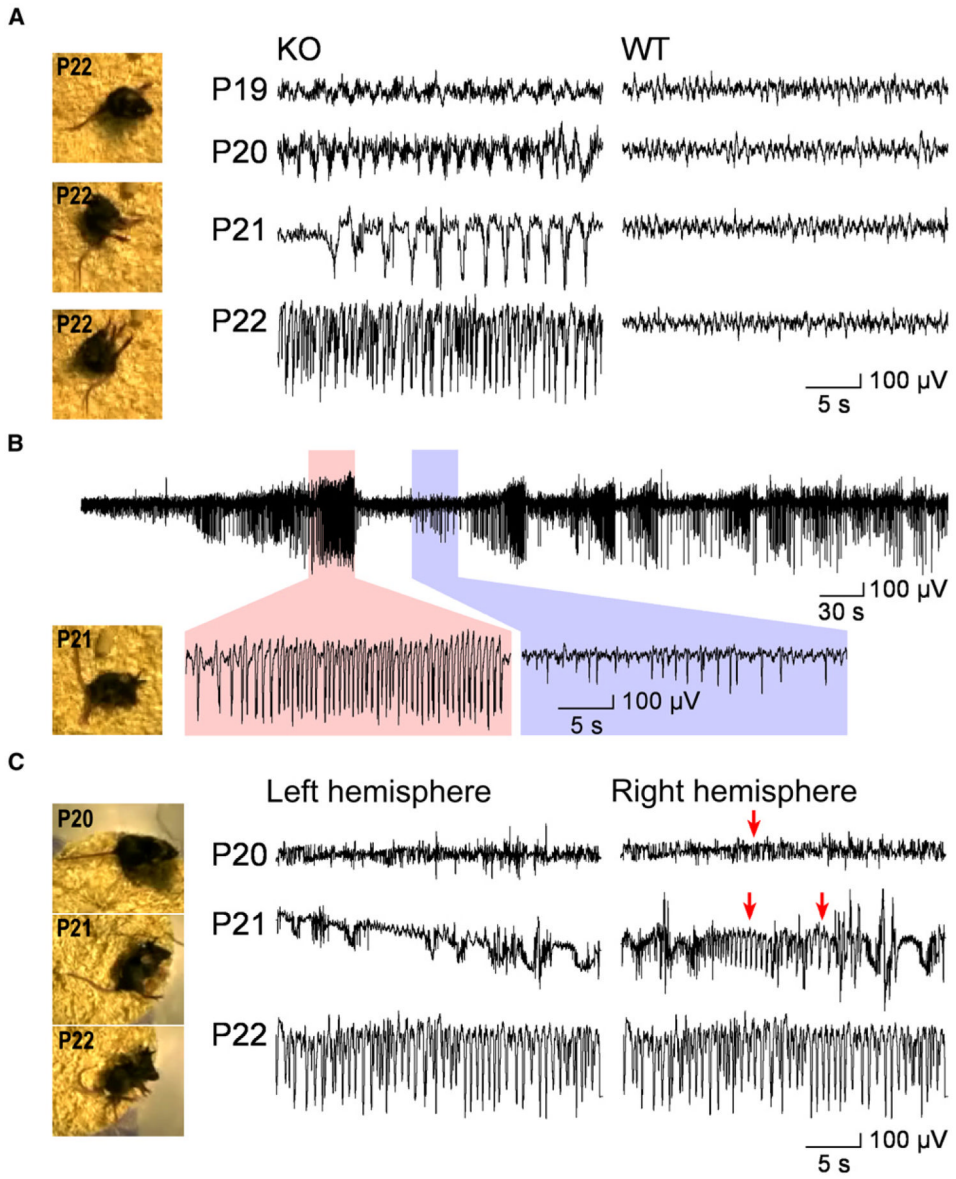

Figure 2. PRG-1 KO Mice Show Epileptic Activity at the End of the Third Week of Life

(A) Preictal events at P20/P21 and ictal activity at P22 during in vivo recordings of a PRG-1 KO mouse (left column; right column: WT littermate). Video images show tonic-clonic seizures of the same KO mice at P22.

(B) Ictal (red) and interictal (blue) periods during in vivo electrographic recording in a P21 PRG-1 KO mouse.

(C) In vivo recording of a PRG-1 KO mouse with implanted electrodes at both hemispheres at P20–P22. Hypersynchronized activity and preictal events can be identified at the right hemisphere around P20/P21 (see arrows); generalized ictal activity is seen over both hemispheres at P22.

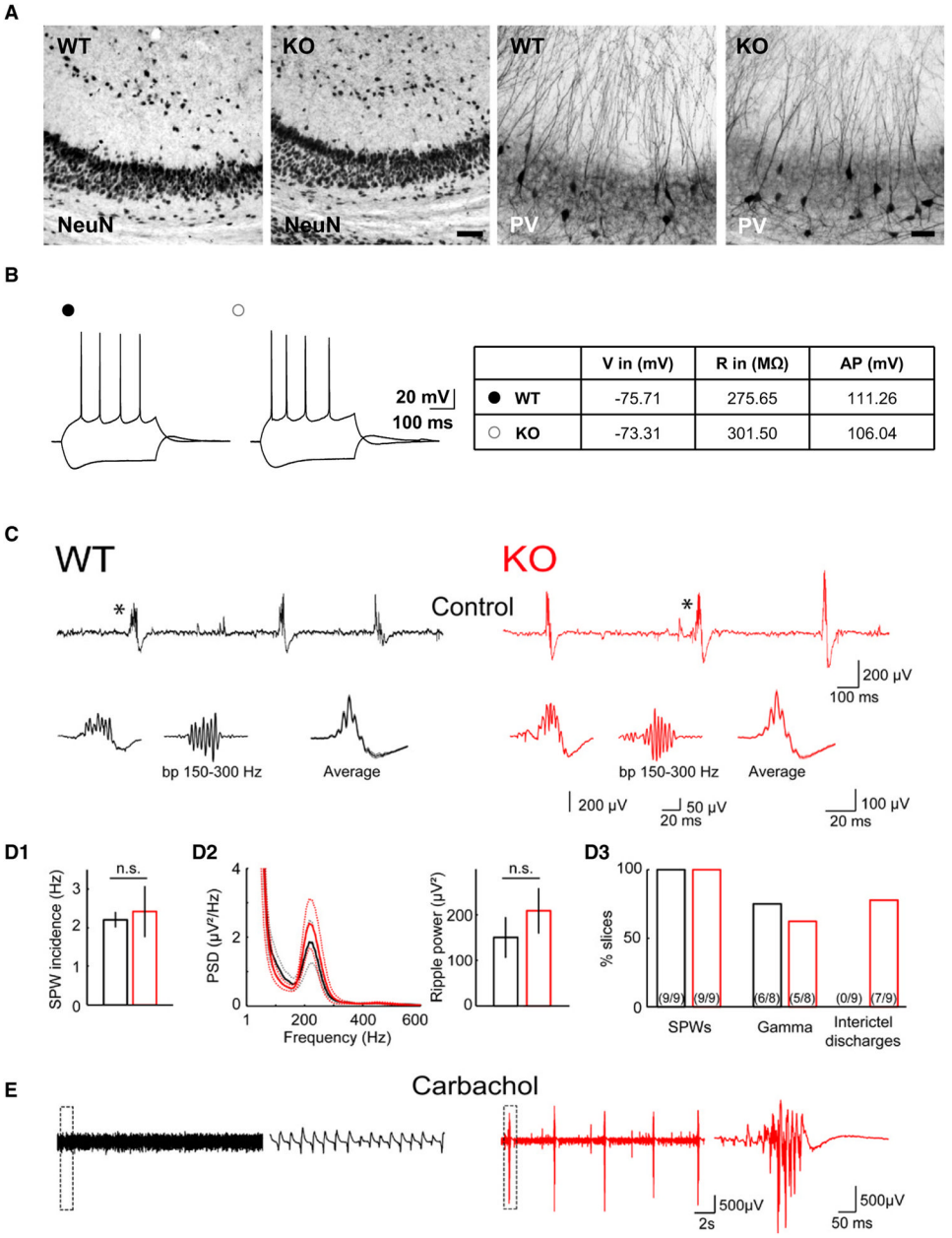

Figure 3. No Evident Structural Changes, but Pathological Network Properties in Hippocampal Slices

(A) Juvenile PRG-1 KO mice (P21) show no changes in morphology as shown by NeuN staining or PV+ interneuron distribution in the hippocampus. The scale bar represents 100 μm (left) and 50 μm (right).

(B) Resting membrane potential, input resistance and action potential height of CA1 pyramidal cells did not vary significantly between WT and PRG-1 KO mice.

(C) Hippocampal sharp wave (SPW)-ripples were expressed in PRG-1 KO slices. Upper traces: example data from CA3 in a WT (black trace) and KO slice (red trace). Below: magnified signals (see asterisks for respective locations in recordings), their band-pass-filtered derivative and SPW peak-triggered averages (±SEM), respectively, of 50 randomly selected SPWs.

(D1) SPW-incidence was not affected in either condition.
(D2) Averaged PSD functions (±SEM) reveal unchanged spectral frequency of ripple oscillation in WT and KO slices. Right: Unaltered ripple power in PRG-$1^{-/-}$.
(D3) Distribution of slices expressing different classes of hippocampal network oscillations: all tested slices expressed SPWs (100%); following carbachol administration, 75% of slices from WT and 62.5% of slices from PRG-$1^{-/-}$ animals displayed gamma activity. Interictal-like discharges were not observed in WT but frequently in KO slices (77.8%). Numbers indicate slice fractions displaying the respective electrographic events.
(E) Example traces showing gamma oscillation from a WT slice (left) and seizure-like events in a KO slice (right) following carbachol administration, with magnified example (box).

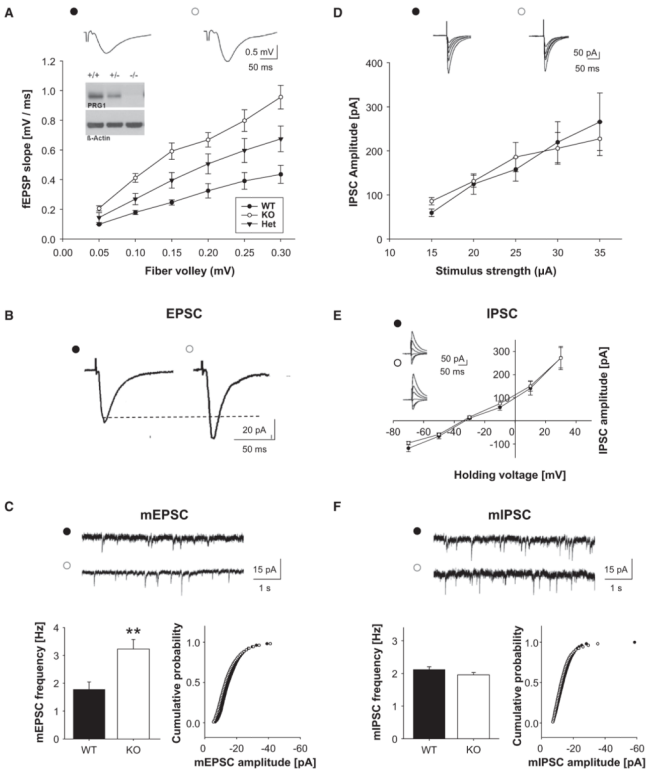

Figure 4. Hyperexcitability in CA1 Neurons in PRG-1 KO Mice

(A) Extracellular fEPSPs were evoked by Schaffer collateral stimulation. fEPSP slope is plotted for WT, PRG-$1^{+/-}$ and PRG-$1^{-/-}$. Increased network excitability is seen for the PRG-$1^{-/-}$ mice (white) compared with WT mice (black). In WT, PRG-$1^{+/-}$ and PRG-$1^{-/-}$ mice, the fEPSP slope increased linearly with increasing fiber volley amplitudes, indicating a gene-dose-dependent effect of PRG-1 reflected in the adjacent western blot of brain homogenates.

(B) Evoked synaptic glutamatergic currents (at similar stimulation intensities and stimulation electrode positions) were enhanced for PRG-1 KO mice compared with WT mice.

(C) A significantly higher mEPSC frequency was observed in PRG-1 KO CA1 pyramidal cells compared to WT cells (left panel), however the amplitude of these events did not significantly vary between the two groups (right panel).

(D) Synaptically evoked IPSCs at different stimulation strengths did not differ between the WT and PRG-1 KO cells.

(E) IV curves of inhibitory currents show no significant difference between the WT and PRG-1 KO cells.

(F) mIPSC frequency (left panel) and amplitude (right panel) did not differ between PRG-1 KO and WT CA1 pyramidal cells.

Data are represented as mean ± SEM, **$p < 0.01$.

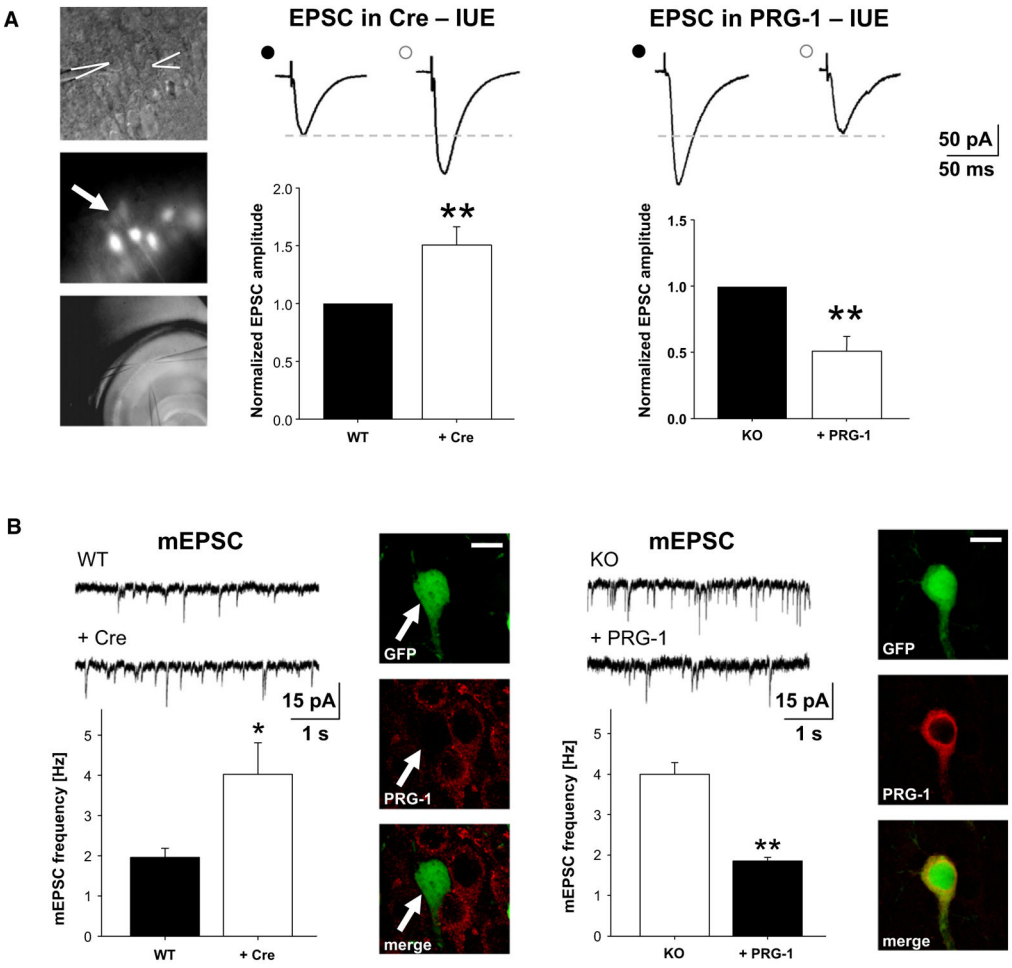

Figure 5. PRG-1 Action in Single CA1 Neurons in Acute Slices

Using in utero electroporation *prg-1* was deleted (GFP^+) in conditional or re-expressed (GFP^+) in constitutive PRG-1 KO mice in a subset of cells.

(A) Left: In simultaneous recordings (upper image) from GFP^+ (KO) and GFP^- (WT, arrow) CA1 pyramidal neurons (middle image) EPSC amplitude (experimental setting: lower image) was significantly increased in KO cells compared to WT cells. Right: In simultaneous recordings from GFP^+ ($PRG\text{-}1^+$) and GFP^- (KO) CA1 pyramidal neurons EPSC amplitude was significantly decreased in PRG-1-expressing cells compared to KO cells.

(B) Left: mEPSCs were recorded from GFP^+ (KO) and GFP^- (WT) cells. Significantly higher mEPSC frequency was observed in the $PRG\text{-}1^{-/-}$ cells compared to WT neurons. Arrow points to GFP^+ cell, in which PRG-1 (red) has been deleted. Right: mEPSC frequency was significantly reduced in the GFP^+ (PRG-1-expressing KO) cells compared to the GFP^- (KO) cells. GFP signal in neurons indicates PRG-1 expression, confirmed by PRG-1 (red) immunolabeling.

Data are represented as mean ± SEM *$p < 0.05$, **$p < 0.01$. The scale bar represents 15 μm.

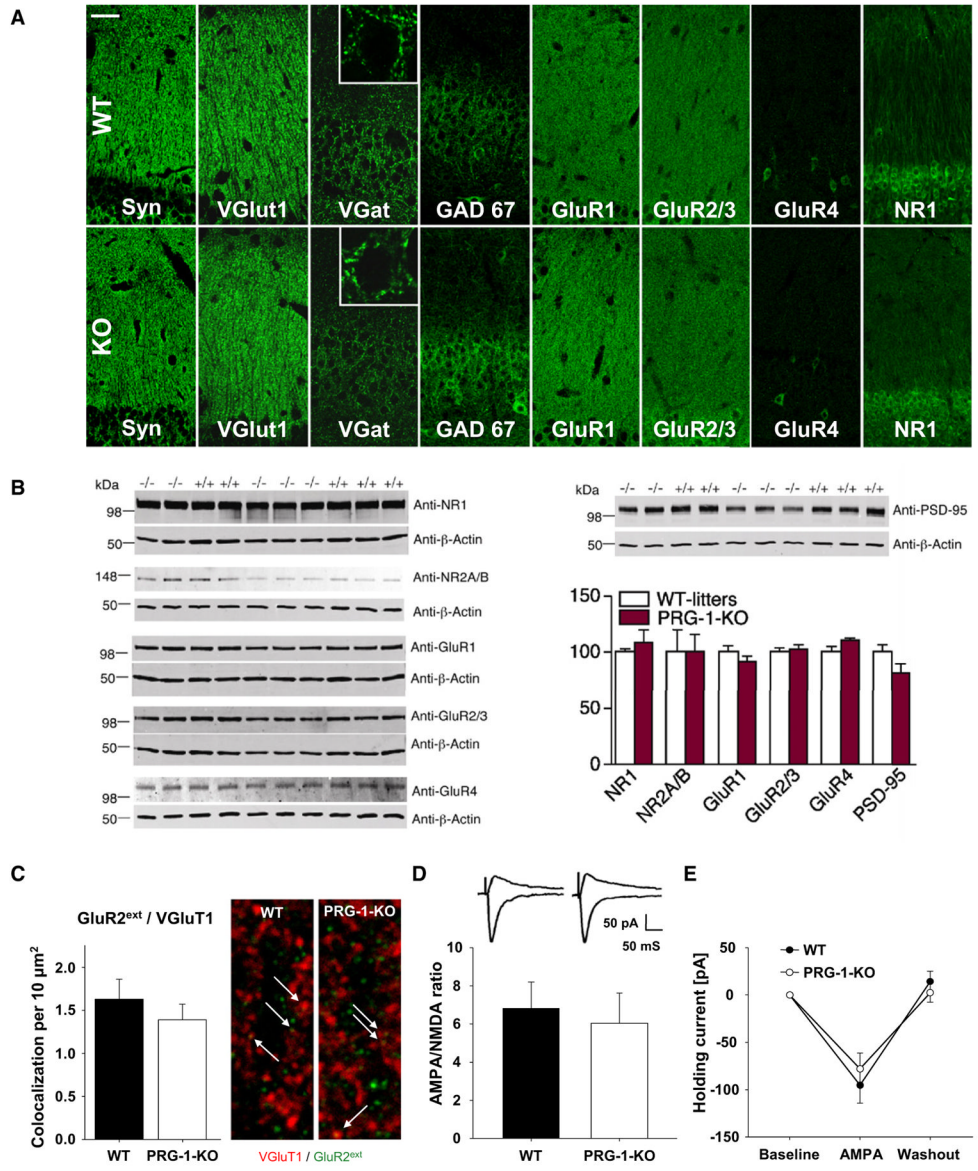

Figure 6. No Evidence for Changes in the Classical Molecular Machinery at the Synapse

(A) Immunofluorescence for presynaptic markers, such as synaptophysin (Syn), vesicular glutamate transporter 1 (VGlut1), vesicular GABA transporter (VGat) and glutamate decarboxylase 67 kDa isoform (GAD67), as well as postsynaptic markers, such as AMPA receptor subunits (GluR1, Glur2/3, GluR4) and the NMDA receptor subunit NR1, do not differ between PRG-1 KO and WT litters. The scale bar represents 50 μm.

(B) Protein analysis of the PSD fraction prepared from PRG-1 KO and WT mice. 2.5 μg of purified PSD fractions were subjected to western blotting to estimate expression levels of NR1, NR2A/B, and GluR1, GluR2/3, GluR4, and PSD-95. Expression of the synaptic proteins were quantified and normalized by the loading control (b-actin) and to the WT.

(C) Immune staining for VGluT1 and GluR2^{ext} on dendrites of CA1 pyramidal cells in WT and PRG-1 KO mice. Arrows indicate colocalization. Stereological analysis of synaptically localized GluR2 revealed no difference between WT (n = 5) and PRG-1 KO (n = 5).

(D) The AMPA/NMDA ratio did not differ between the WT and PRG1-KO mice.

(E) The holding current changes on AMPA (50 nM) wash-in did not differ significantly between the WT and PRG-1 KO mice.
Data are represented as mean ± SEM.

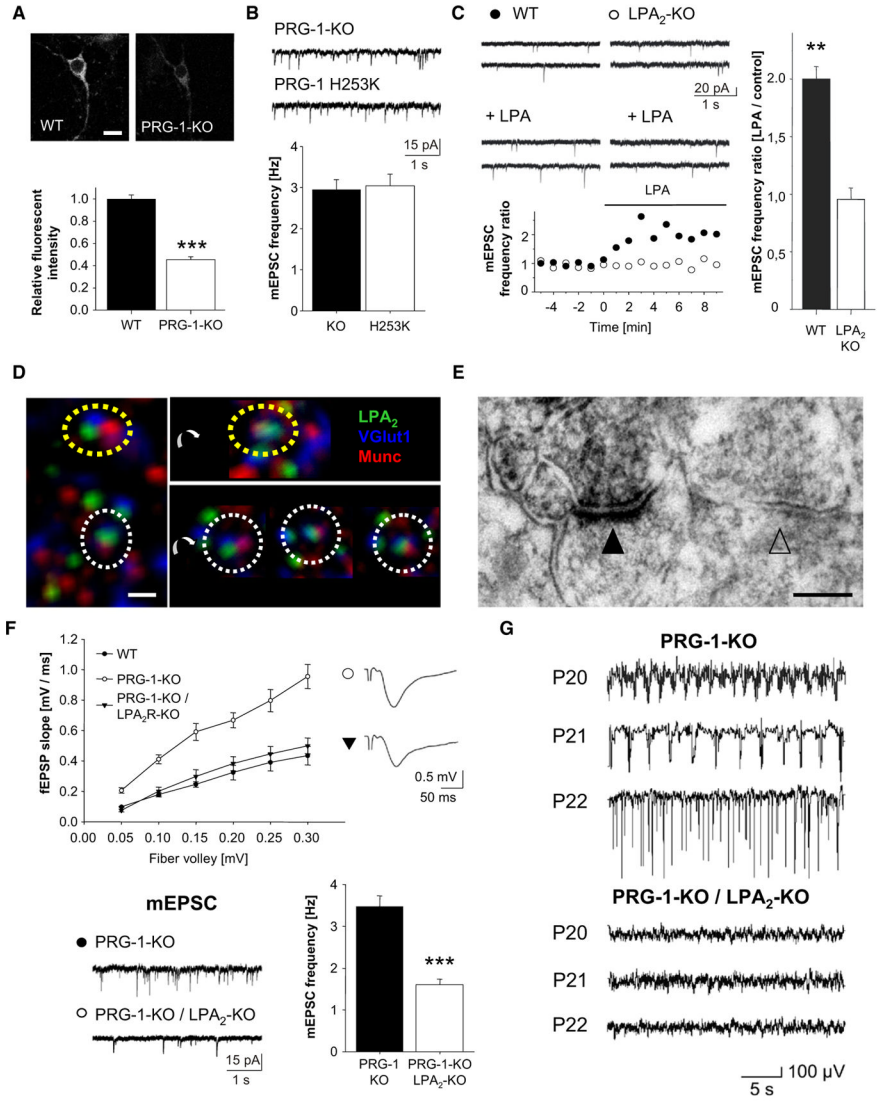

Figure 7. PRG-1 Influences Phospholipid Signaling

(A) NBD-PA uptake experiments in primary neurons revealed significantly lower fluorescence intensity in KO cells compared to WT litter cells, indicating reduced lipid uptake (the scale bar represents 10 μM).

(B) Mutated PRG-1 (H253K) lacking the ability to interact with phospholipids was expressed in a subset of cells (GFP^+) in PRG-1 KO animals using in utero electroporation. mEPSC frequency at P21 was not reduced to WT levels in PRG-1 (H253K)-expressing neurons after electroporation of the WT *prg-1* construct (see Figure 5).

(C) mEPSC frequency rapidly increased in CA1 pyramidal neurons after application of 10 μM LPA, but not in LPA_2 receptor-deficient animals (LPA_2-R-KO). For the analysis, the mEPSC frequency of each analyzed neuron was averaged for the last four minutes under control conditions and in steady state after LPA treatment, and these values then compared.

(D) 3D reconstruction of a presynaptical terminal positive for the LPA_2-R, the presynaptic glutamatergic marker VGlut1 and the active zone marker Munc13-1 (the scale bar represents 0.5 μm).

(E) Ultrastructural analysis of the LPA_2-R localization revealed a strong DAB signal on the presynaptic side of an asymmetric, presumably glutamatergic synapse (arrowhead). Two adjacent axons display a positive signal underlining the presynaptic LPA2-R localization. In contrast, no LPA_2-R signal was found in symmetric, presumably inhibitory synapses (open arrowhead) (the scale bar represents 200 nm).
(F) Normal network excitability is seen in PRG-1 KO/LPA_2-R KO $^{-/-}$ animals when compared to the PRG-1 KO mice. In contrast to PRG-1 KO mice, double KO animals showed fEPSP slopes similar to WT animals. mEPSC frequency in CA1 pyramidal neurons in hippocampus from double KO mice also returned to WT levels and did not show the increase seen in PRG-$1^{-/-}$ animals.
(G) In vivo recordings of double KO animals did not display the hypersynchronized activity around P21 seen in PRG-$1^{-/-}$ mice of same age.
Data are represented as mean ± SEM, **$p < 0.01$, ***$p < 0.001$.